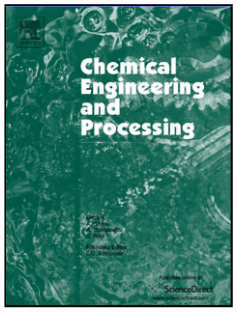

Title: Experimental and computational investigation of heat transfer in a microwave-assisted flow system

Authors: Spyridon Damilos, Anand N.P. Radhakrishnan, Georgios Dimitrakis, Junwang Tang, Asterios Gavriilidis

PII: S0255-2701(18)31507-1
DOI: https://doi.org/10.1016/j.cep.2019.107537
Article Number: 107537

Reference: CEP 107537

To appear in: *Chemical Engineering and Processing*

Received date: 10 December 2018
Revised date: 2 April 2019
Accepted date: 19 May 2019

Please cite this article as: Damilos S, Radhakrishnan ANP, Dimitrakis G, Tang J, Gavriilidis A, Experimental and computational investigation of heat transfer in a microwave-assisted flow system, *Chemical Engineering and Processing - Process Intensification* (2019), https://doi.org/10.1016/j.cep.2019.107537

Experimental and computational investigation of heat transfer in a microwave-assisted flow system

Spyridon Damilos[1], Anand N. P. Radhakrishnan[1], Georgios Dimitrakis[2], Junwang Tang[1] and Asterios Gavriilidis[1]

[1]Department of Chemical Engineering, University College London, Torrington Place, London, WC1E 7JE, United Kingdom

[2]Department of Chemical and Environmental Engineering, Faculty of Engineering, University of Nottingham, University Park, Nottingham, NG7 2RD, United Kingdom

Corresponding authors: georgios.dimitrakis@nottingham.ac.uk, a.gavriilidis@ucl.ac.uk

Graphical abstract

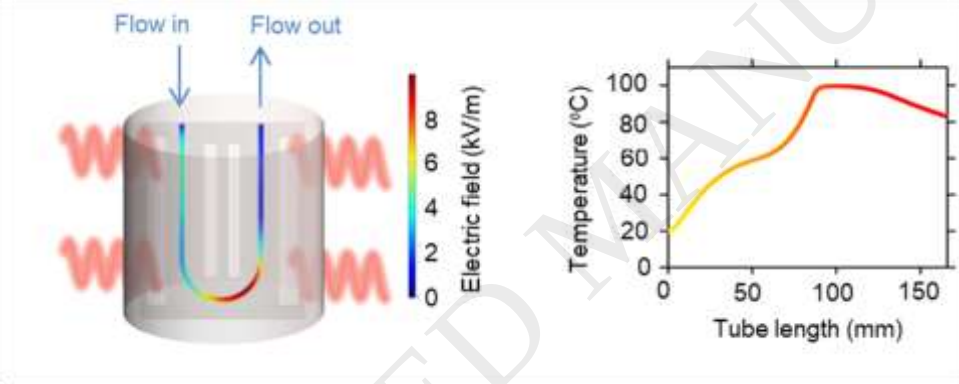

Highlights

- A CFD model is developed to simulate microwave heating in a millifluidic channel.
- The effect of process parameters on the temperature profile are investigated.
- Satisfactory agreement between modelling and experiments is obtained.

Abstract

Microwave technology is gaining popularity as a tool for chemical process intensification and an alternative to conventional heating. However, in flow systems non-uniform temperature profiles are commonly encountered and hence methods to characterise and improve them

are required. In this work, we studied the effects of various operational parameters - microwave power, inlet flow rate, tube orientation and pressure - on the electric field and temperature profiles of water flowing in a PTFE tube (2.4 mm internal diameter), placed in a commercial single-mode microwave applicator. A finite element model was developed to estimate the longitudinal temperature profiles and the absorbed microwave power, while *in situ* temperature monitoring was performed by a fibre optic probe placed at multiple locations inside the tube. The water temperature inside the tube increased by increasing the microwave power input and temperature profiles stabilised beyond 20 W, while the percentage absorbed microwave power showed the inverse trend. When changing the tube orientation or decreasing the inlet flow rate, microwave absorption decreased significantly. When the pressure was increased to 2.3 bara, water temperature increased by ~ 20 ^{o}C. Results from this study provide valuable insights on achievable temperature profiles and energy efficiency of microwave-assisted flow synthesis systems.

Keywords: Microwave heating, Continuous flow, Heat transfer, Modelling

1. Introduction

Microwave heating has been studied over the past decades as an alternative to conventional heating. The main advantages of microwave technology are rapid heat transfer, selective heating (depending on the dielectric properties of the medium), superheating of the solvents and providing a renewable and sustainable heating source, since electricity can be sourced from renewable means [1]. These advantages have made microwave heating attractive in various areas including organic and polymerisation reactions [2-4], bioelectromagnetic studies [5], food processing [6], nanoparticle synthesis [7, 8], catalytic processes [9, 10], adsorption processes [11], reactive distillation [12] and microreactor processing [13-15]. Microwave heating is generally described as volumetric heating in nature, as it usually takes place over the entire workload volume and depends on the dielectric properties of the medium, which are also a function of temperature and frequency [16]. Therefore, for certain conditions and dielectric property values, microwave energy is deposited directly into the entire workload volume and the mechanism is not driven by conduction and convection, as in conventional heating [8, 17]. Microwave and conventional heating can be combined by exploiting the rapid energy transfer of microwave power and the readily-controllable heat exchange by conventional heating to maintain the targeted temperature [10]. An interesting feature of this technology is the inverse temperature profile inside the heated medium [2], which is due to the temperature gradient between the medium and the container and the heat loss to the surrounding medium. When the container dimensions are smaller or

comparable to the microwave penetration depth, the cross sectional temperature distribution could be uniform. Microwave heating has also received attention for large-scale or industrial systems, aiming to intensify chemical processes [11, 18]. This task requires optimisation of the microwave cavity for the targeted application, along with the microwave generators and the available reactors, to couple the electromagnetic phenomena with the heat generation in the scaled-up system [18].

Temperature distribution in a medium subject to microwave heating depends on the electromagnetic field. In the case of micro-reactors and milli-reactors, the penetration depth - the distance from the medium surface, to the point where the microwave power drops to ~ 37 % of the initial value at the surface - is much larger than the tube diameter [19]. Thus, microwave heating can be assumed to be homogeneous in the cross section and the spatial distribution of the electromagnetic field is described by Maxwell's equations. Several studies were conducted in the past implementing computational modelling in order to simulate the temperature profile of solid materials [6], liquids (in batch or in flow) [17, 20] and liquid-solid particle systems [21]. Modelling studies of microwave heating use either the finite element method (FEM) [17, 20, 22-24] or the finite-difference time-domain (FDTD) [25, 26] techniques to couple and simultaneously solve the electromagnetic field, heat transfer and fluid flow to describe the system.

Salvi et al. [22] compared results obtained by FEM modelling with experimental results for continuous flow of water in a PTFE tube placed inside a TE10 microwave applicator. Modelling overestimated the temperature of the medium, resulting in 5 – 20 ^{o}C discrepancies between experimental and computational results at the edges of the tube. These discrepancies were attributed to the no-slip boundary conditions resulting in zero fluid velocity at the tube walls, intensifying the electric field and thereby, the final temperature. However, another possible reason explaining those discrepancies was the insufficient meshing of the domains [22, 27]. Yousefi et al. [28] simulated the temperature profiles of water under continuous flow conditions in a vertical tube, undergoing microwave heating through a rectangular waveguide. They coupled heat transfer and fluid flow physics and discussed the effects of the inlet water velocity and applicator dimensions on the temperature profiles. Tuta and Palazoğlu [24] coupled Maxwell's equations, Fourier's heat transfer equation and Navier-Stokes equation to optimise the microwave energy uptake to achieve greater and more uniform temperature increase of fluids in a pilot-scale, continuous flow, coiled PTFE tube under microwave heating. Varying dielectric properties and the presence of secondary flow were included in their studies. Robinson et al. [29] investigated the microwave dissipation on the walls of a microwave absorbing vessel (such as silicon carbide), resulting in elevated temperatures in the medium, as opposed to "microwave

transparent" vessels. From previous studies [17, 23, 30, 31] it is evident that the temperature profile depends on the geometry, dimensions and materials of the reactor, as well as reactor position and flow rate of the medium. Morgan et al. [31] described the presence of electric field depolarisation on a Teflon microfluidic chip on horizontal and perpendicular orientation, focussing on the reactor and medium characteristics rather than liquid flow. In their analysis they altered the orientation of the chip and observed higher heating efficiency when the electric field was parallel to the long dimension of the straight channels of the chip.

In this work, we investigated numerically and experimentally the effects of various operational parameters on the temperature profile in a milli-scale tube placed in a commercial single-mode microwave applicator. We developed an FEM model that simulated the temperature and electric field profiles along the tube length and the absorbed microwave power and used it to study the effect of various operating parameters.

2. Experimental section

2.1 Experimental setup

A commercial single-mode microwave applicator (Discover SP, CEM) was used for microwave generation. A U-shape tube of total volume 0.75 ml (inner diameter, I.D. 2.4 mm, outer diameter, O.D. 3.175 mm, length: 165 mm) on a flat-plate support structure was placed into the microwave cavity, allowing entrance and exit of the flowing medium from the top. The tube and the support structure were made of polytetrafluoroethylene (PTFE), which is considered a "microwave transparent" material due to its low dielectric loss factor. The input power ranged from 5 W to 35 W. The effect of the U-shape tube orientation on the temperature profile was studied by placing the support structure parallel and perpendicular to the microwave port, hereafter referred as "parallel-to-port" and "perpendicular-to-port", respectively. The flow rates of water were 0.5 ml/min, 0.7 ml/min and 1.5 ml/min, resulting in mean residence times of ca. 0.5-1.5 min, and were controlled using syringe pumps (Legato 270P, KD Scientific) with 25 ml glass syringes (25MDR-LL-GT, Scientific Glass Engineering). The pressure inside the tube was regulated with a backpressure regulator (maximum 4 barg, Swagelok). Immediately after switching on the microwave power, the temperature rapidly increased and reached the target temperature, but we allowed extra time before taking the temperature readings (5 min) in order to ensure there were no temperature fluctuations over time. Temperature was monitored via a fibre optic temperature sensor (O.D. 1.7 mm, T1s, Neoptix) with direct temperature measurements at 5 different positions throughout the tube length. The fibre optic sensor was inserted from the tube outlet, to avoid flow disturbances and measurement inaccuracy [17]. Temperature

measurements were performed at 36 mm (point 1), 70 mm (point 2), 83 mm (point 3), 95 mm (point 4) and 135 mm (point 5) from the tube inlet (point 0) (see Figure 1).

2.2 Materials and methods

Ultra-pure water (15 MΩ·cm) was used for all experiments. PTFE tubes (1 mm I.D., VICI Jour) were used for all fluidic parts and polyether ether ketone (PEEK) ferrules and fittings were used for all connections. Dielectric constant and dielectric loss of water were experimentally evaluated for the temperature range 20-95 ^{o}C at atmospheric pressure, following the methodology previously described in literature [32], and are shown in Table S1 (Supplementary Information). The measurements showed that the water dielectric properties were almost constant for each measured temperature between 2.45 GHz and 2.47 GHz, which is within the magnetron specifications. PTFE was assumed to be microwave transparent in the studied conditions ($\varepsilon_{r,PTFE} = 2.1 - 0j$) [16].

3. Mathematical model development

3.1 Geometry and discretisation of the cavity

The model geometry is a representation of the geometrical features of the single-mode microwave applicator, as shown in Figure 1. The microwave generator utilised a magnetron set at 2,460 MHz (+/- 10 MHz) having microwave power range 1-300 W. The computational modelling considered only the cavity and the tube with the support structure. The cavity was made of stainless steel and contained a PTFE protective ring. Within the metallic cavity there were 6 rectangular ports, providing uniform electromagnetic field to the load placed in the cavity. The geometry of the applicator and the tube are displayed in Figure 1.

The analysis of the electromagnetics and heat transfer in the system was carried out in COMSOL Multiphysics software (v.5.3a, COMSOL Inc.), similar to the methodology described by Sturm et al. [20], and computational analysis was divided into two steps. A diagram of the interconnected computational steps is shown in Figure 2. In the first step, the Electromagnetic Waves module was solved for the electric field throughout the length of the tube, by keeping the dielectric properties (dielectric constant ε' and dielectric loss ε'') of water constant at 20 ^{o}C (Figure 2, Step 1) including all domains (the metal cavity, the contained PTFE protective ring, air, the PTFE support structure, the PTFE tube and the water flowing inside the tube). No fluid flow was taken into account at this stage. Due to the difference in transmitted and reflected microwave energy [20] and the lack of control over matching impedance, a parametric sweep over the magnetron frequency was conducted under the respective experimental conditions. The parametric sweep was performed over the frequency of the magnetron which varied between 2,450 MHz and 2,470 MHz at a 5

MHz step, for each microwave power. In the second step, the Heat Transfer and the Laminar Flow modules were coupled for the computation of the temperature profile of water in the tube, for the corresponding laminar flow conditions (Figure 2, Step 2). Heat losses via conduction from the water to the tube wall and support structure, as well as via radiation and natural convection were also taken into account. The heat source across the tube length was calculated based on the electric field profile evaluated in the Electromagnetic Waves module (Step 1). Varying electric field profiles for each set of microwave power and respective magnetron frequency (from the parametric sweep) were obtained in Step 1 and used in Step 2. The magnetron frequency which resulted in the highest power absorption was estimated by comparing the experimental and computational results of the temperature for each set of frequencies; the frequency value at which we observed maximisation of the absorbed microwave power and minimum discrepancy between experimental and computational results was denoted as the optimum magnetron frequency, and was found to be 2.47 GHz for all cases. For the three different flow rates studied, the Reynolds number for water at 20 ^{o}C was in the range 4.96-14.9, confirming the existence of laminar flow in the U-shape tube.

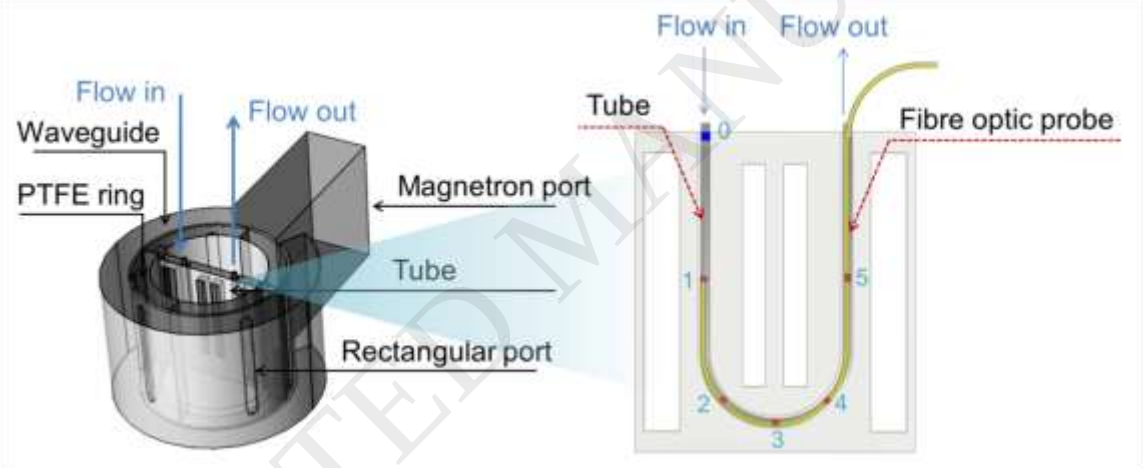

Figure 1. (Left) schematic of inner parts of the CEM Discover SP microwave applicator. (Right) the tube with the PTFE support structure. The tube is displayed in grey colour and the fibre optic temperature probe is displayed in yellow colour. The blue mark indicates the tube inlet (point 0) and the red marks indicate the points of temperature measurements made by inserting the probe from the tube outlet (point 1: 36 mm, point 2: 70 mm, point 3: 83 mm, point 4: 95 mm, point 5: 135 mm from tube inlet). Images are not to scale.

Meshing for Step 1 was set at “Coarse” (element size max: 16.5 mm, min: 5.07 mm) for the metal cavity, the contained PTFE protective ring and the air domains, “Fine” (element size max: 6.71 mm, min: 1.27 mm) for the PTFE support structure and the PTFE tube, and “Extra fine” (element size max: 2.91 mm, min: 0.19 mm) for the water flowing inside the tube, resulting in 1,442,208 elements. The simulations were carried out in “Frequency Stationary” mode, as steady state conditions were assured during the experimental procedure. Meshing

for Step 2 was set at “Fine” (element size max: 6.71 mm, min: 1.27 mm) for the PTFE support structure and the PTFE tube, and “Extra fine” (element size max: 2.91 mm, min: 0.19 mm) for the water flowing inside the tube, resulting to 356,826 elements. The computer used was equipped with an Intel® Xeon® CPU E5-2637 V3, at 3.50 GHz (2 processors), with 192 GB RAM, running on 64-bit Windows® Server 2016. Total simulation time was ca. 26 min for both Step 1 and Step 2. Calculations using finer meshing showed that results were mesh-independent.

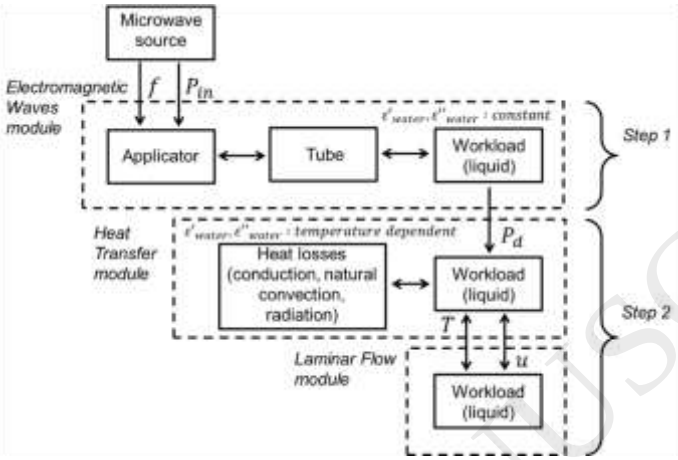

Figure 2. Diagram of the interconnected modules and variables for the two steps of the Finite Element Method model developed in COMSOL Multiphysics. In Step 1, the Electromagnetic Waves module computed the electric field profile throughout the tube length. In Step 2, the Heat Transfer and Laminar Flow modules were coupled for the computation of temperature profile. The microwave power density in Step 2 was calculated as a function of the electric field output from Step 1.

3.2 Electromagnetic Waves module

The temperature distribution in a material that is being subject to microwave heating depends on the electromagnetic field. The electric field profile given by the Helmholtz representation of Maxwell’s electromagnetic field equations is described by [33]:

$$\nabla^2 \boldsymbol{E} + \varepsilon_r \left(\frac{2\pi f}{c}\right)^2 \boldsymbol{E} = 0 \qquad (1)$$

where $\boldsymbol{E}$ is the electric field vector of the time-harmonic oscillating microwave field, f is the frequency of the electromagnetic field, c is the speed of light in vacuum and ε_r is the relative complex permittivity, which consists of the dielectric constant ε' and dielectric loss ε'' ($\varepsilon_r = \varepsilon' - j\varepsilon''$). ε' is dependent on the material and describes its potential to store the microwave energy and thus be polarized by the electromagnetic field. ε'' describes the efficiency of the material in converting electromagnetic energy into heat. The higher the dielectric loss, the higher is the amount of electromagnetic energy which is converted into heat (i.e., leading to

a higher final temperature). The microwave power density in the medium is described by [16, 20]:

$$P_d = 2\pi f \varepsilon_o \varepsilon'' |\boldsymbol{E}|^2 \quad (2)$$

where ε_o is the electric permittivity of vacuum and $|\boldsymbol{E}|$ is the electric field intensity.

The input parameters for the Electromagnetic Waves module were the input microwave power and the magnetron frequency and the output was the electric field profile. The model assumptions and boundary conditions for Step 1 are included in Section 3 in the Supplementary Information.

3.3 Heat Transfer module

The heat transfer in the medium (workload) was calculated using the Heat Transfer module in Step 2 (Figure 2). Temperature rise in the medium depends on the coupling of Maxwell's equations and Fourier's heat transfer equation [26, 28]:

$$\rho C_p(\boldsymbol{u} \cdot \nabla T) = \nabla Q + P_d \quad (3)$$

The term on the left hand side describes the contribution of convection to heat transfer. The first term on the right hand side describes the contribution of conduction to heat transfer and the second term is the heat generation in the medium. The heat flux through the tube wall and support structure is given by Equation 4, while the heat loss to the ambient environment due to natural convection and radiation is given by Equation 5:

$$Q = k\nabla T \quad (4)$$

$$Q = h_{air}(T_{air} - T) + \varepsilon\sigma({T^4}_{air} - T^4) \quad (5)$$

where ρ is the density, C_p is the specific heat capacity, Q is the heat flux, $\boldsymbol{u}$ is the fluid velocity field vector inside the tube, T is the temperature, P_d is the microwave power density, k is the thermal conductivity, T_{air} is the air and ambient temperature, h_{air} is the heat transfer coefficient for natural convection, ε is the surface emissivity and σ is the Stefan–Boltzmann constant. The water thermal properties and other parameters used in the model are provided in Tables S3 and S4 in the Supplementary Information.

3.4 Laminar Flow module

The fluid flow profile was computed using the Laminar Flow module, as shown in Step 2 (Figure 2), by solving the momentum balance equation (incompressible Navier–Stokes equation) described by [34]:

$$\rho[\boldsymbol{u} \cdot \nabla \boldsymbol{u}] - \eta\nabla \cdot [\nabla \boldsymbol{u} + (\nabla \boldsymbol{u})^T] + \nabla p = 0 \quad (6)$$

and the continuity equation for incompressible fluids:

$$\rho(\nabla \cdot \boldsymbol{u}) = 0 \quad (7)$$

where ρ is the density of the medium, η is the dynamic viscosity, $\boldsymbol{u}$ is the fluid velocity field vector and T is the temperature. The first term in the momentum balance equation is the inertial forces, the second term is the viscous forces and the third term is the pressure gradient. No slip boundary condition was set on the inner tube wall in contact with the liquid. Temperature and fluid velocity were obtained via the coupled calculation in Step 2 between Heat Transfer and Laminar Flow module (Figure 2). The values of the various parameters used in the simulations are given in Table S3 in the Supplementary information.

4. Results and Discussion

4.1 Influence of process parameters on temperature profile

The microwave field is influenced in general by the dielectric properties of the materials used, the level of the microwave power and the flow conditions. These interactions result in different temperature profiles throughout the tube length which affect the reaction rates of reactive processes. Microwave heating is related to the workload inside the cavity, therefore microwave power and flow rate were investigated for their effect on the temperature profile over the tube length. Due to the perturbation of the electric field by the geometrical characteristics of the cavity and the tube, we varied the orientation of the tube with respect to the microwave port of the applicator. Finally, the effect of system pressure on dielectric properties and temperature profiles was investigated, since elevated pressures, commonly used in chemical syntheses, increase the boiling point of the liquid in the system.

4.1.1 Effect of microwave power on temperature profile

Figure 3 shows the temperature profile in the centre of the tube along its length, at different input microwave powers. All experiments were conducted at atmospheric pressure and for that reason maximum temperature achieved experimentally was around 100 ^{o}C (boiling point of water). For the cases of 25 W, 30 W and 35 W, the maximum temperature reached 100.8 ± 0.5 ^{o}C, exceeding that of water boiling point. This could be attributed to the superheating effect of water under a microwave field, due to lack of bubble nucleation sites [35, 36]. Increasing microwave power from 5 W to 35 W resulted in temperature profiles with similar trends, despite the higher energy intensity. Comparing the experimental temperature profiles between 5 W to 15 W, an upward trend for the same measurement positions can be observed (Figure 3a). Close to the outlet of the tube (at point 5), there was a ~ 30 ^{o}C increase when the microwave power increased from 5 W to 15 W. However, when increasing microwave power from 20 W to 35 W, there was no further temperature increase

at the same measurement positions (Figure 3b). This behaviour can be explained by the absorbed microwave power being similar at different microwave power inputs, as described in Section 4.2.2. Note that for 15 – 35 W input power, the temperature at point 5 varied between 87-89 ^{o}C and it was lower than the maximum temperature measured in the middle of the tube (Figure 3a and 3b). Reasons for the observed temperature drop were the heat losses via conduction (to the exterior of the PTFE tube and the support structure), radiation and natural convection, as well as the lower electric field intensity towards the outlet of the tube [37]. Another factor contributing to this temperature drop was phase change. As water reached the boiling point in the middle of the tube, vapour bubbles formed, which have different dielectric properties than liquid water [38], and reflected the microwave radiation, subsequently leading to perturbation of the electric field [31].

Although there was satisfactory agreement between experimental and computational results, discrepancies were observed. Following the parametric study on the magnetron frequency, the optimum magnetron frequency was 2.47 GHz, resulting in maximum microwave power absorbance and minimum difference between experimental and computational results on the temperature profile. The FEM model underestimated the temperature close to the inlet (point 1) by ~ 2.5 ^{o}C up to 25 W and it increased in the middle of the tube (points 2 – 4) varying between 1.5 ^{o}C (30 W) to 25 ^{o}C (15 W). These discrepancies were not constant throughout the tube length, but varied with microwave power and position in the tube. They could be related to the characteristic non-uniform electromagnetic field scattering along the tube length inside the microwave cavity, which leads to non-isothermal heating. Additionally, they could be associated with unstable magnetron behaviour due to overheating and the effect of reflected microwaves on applicator cavity and the magnetron [20, 30]. Salvi et al. [22] observed that FEM modelling overestimated the temperature of the medium both at the centre and the walls of the tube, and attributed the latter to high electromagnetic density as a result of zero liquid velocity (no slip boundary condition) imposed on the walls. It is worth noting that the 3-dimensional electric field intensity inside the water phase was utilised in our analysis for improved prediction of the temperature profile. Regarding phase change and subsequently bubble formation, Salvi et al. [22] modified their model to account for this phenomenon and their model seemed to over-predict the temperature at higher temperature regions. In our study, we accounted for phase change by assuming the dielectric loss of water $\varepsilon'' = 0$ when the temperature reached 100 ^{o}C at 1 bara, and therefore no microwave absorption occurred. Experimentally, bubbling was observed from 95 ^{o}C and hence ε'' values were measured only up to 95 ^{o}C (see Table S1), and for the FEM modelling a linear interpolation between ε'' at 95 ^{o}C and $\varepsilon'' = 0$ at 100 ^{o}C was performed by COMSOL.

Cherbański and Rudniak [23] also discussed the sources of the discrepancies between experimental and computational results. According to their study, the shift in the magnetron frequency was the primary parameter affecting the experimental results. The type of the fibre optic sensor and the assumption of constant dielectric properties could enhance the observed discrepancies. However, Robinson et al. [32] examined the effect of a fibre optic probe in batch conditions, showing negligible changes on electric field distribution because of the probe. We compared the simulated temperature profiles with and without the fibre optic, and even though the fibre optic affected the electric field intensity locally, the temperature profile was not affected (see Figures S2 – S3, Supplementary Information).

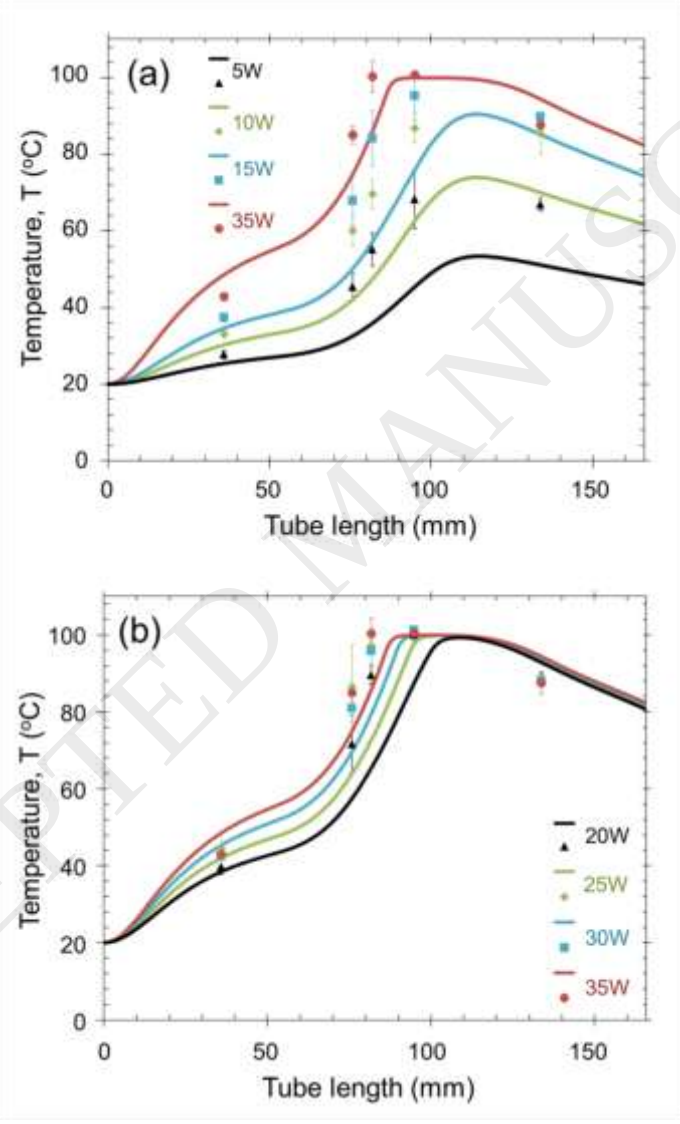

Figure 3. Experimental and computational results of the temperature profile inside the tube, when varying microwave power (a) 5-35 W, (b) 20-35 W. Flow rate, 0.7 ml/min; tube orientation: parallel-to-port; system pressure, 1 bara; frequency, 2.47 GHz (marks: experimental results; lines: computational results). Error bars correspond to the standard deviation of three experimental measurements at each point. Computational results correspond to the temperature profile in the centre of the tube (water domain).

4.1.2 Effect of tube orientation on temperature profile

Tube orientation was studied by placing the tube assembly parallel (parallel-to-port) and perpendicular (perpendicular-to-port) to the microwave port, as shown in Figure 4.

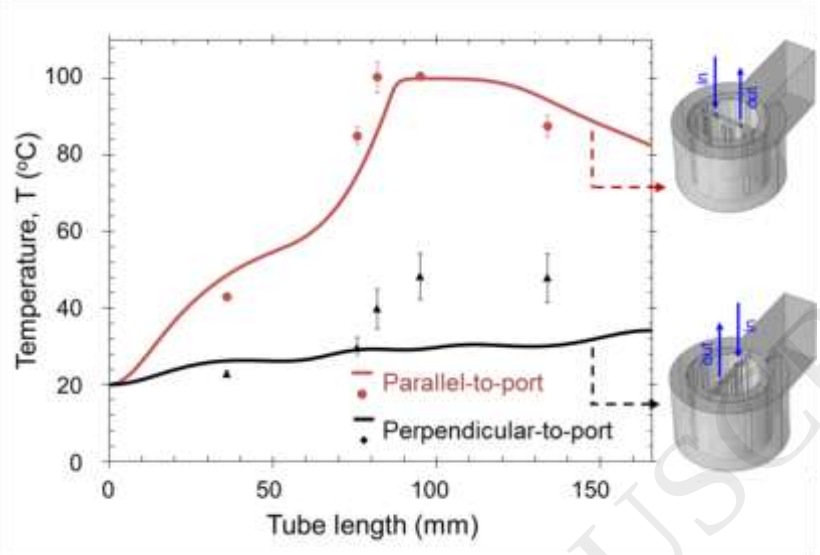

Figure 4. Experimental and computational results of the temperature profile inside the tube, when varying the tube orientation. Flow rate, 0.7 ml/min; microwave power, 35 W; system pressure, 1 bara; frequency, 2.47 GHz (marks: experimental results; solid lines: computational results). Error bars correspond to the standard deviation of three experimental measurements at each point. Computational results correspond to the temperature profile in the centre of the tube (water domain).

The temperature profile inside the tube was affected by the orientation of the tube with respect to the microwave port, leading to a 50 °C difference in the maximum temperature reached (Figure 4). Morgan et al. [31] discussed the effect of the depolarisation of the electric field when the microwave radiation crosses the boundaries of materials of different dielectric properties, as well as its dependence on the material geometry and orientation in the cavity. In our study, the maximum unperturbed electric field intensity was observed in the centre of the applicator (Figure 5a) and for this reason the tube was placed in the centre of the cavity, similar to previous studied microwave-assisted syntheses for maximum microwave power absorbance [5]. Due to the geometrical characteristics of the cavity of the Discover SP – considering the 6 rectangular ports on the metallic cavity – both the straight inlet and the outlet parts of the U-shape tube were always parallel to the sidewalls of the cavity whereas a minor area of the curved part was parallel to port. Therefore, the observed differences on the temperature profile and heating rate were the result of the interaction of the U-shape tube with the minima and maxima of the resonant electric field. These interactions of the tube with the electric field affected the temperature profile experienced by

the liquid. Figure 5b and 5c show the different electric field profiles inside the tube when placed in parallel-to-port and perpendicular-to-port orientation, respectively.

The microwave power density was one order of magnitude higher when the tube was placed parallel-to-port (Figure 6a), instead of perpendicular-to-port (Figure 6b). In parallel-to-port orientation, the maximum power density was located at the curved part of the tube, which was parallel to the applied field, resulting in the maximum observed temperature. Considering the electric field profiles and the microwave power density along the tube, changing the tube orientation to perpendicular-to-port position resulted in significant depolarisation which lessened the heating efficiency, as described by Morgan et al. [31]. Experimental results of the temperature profile for perpendicular orientation showed a steep increase in the middle of the tube, while the temperature profile obtained from the simulations for the same conditions showed a steady temperature increase throughout the tube length (see Figure 4). The temperature difference between experimental and computational results in the perpendicular-to-port orientation, was between 0.3 – 19.0 ^{o}C, which was comparable to that in the parallel-to-port orientation (0.7 – 14.0 ^{o}C).

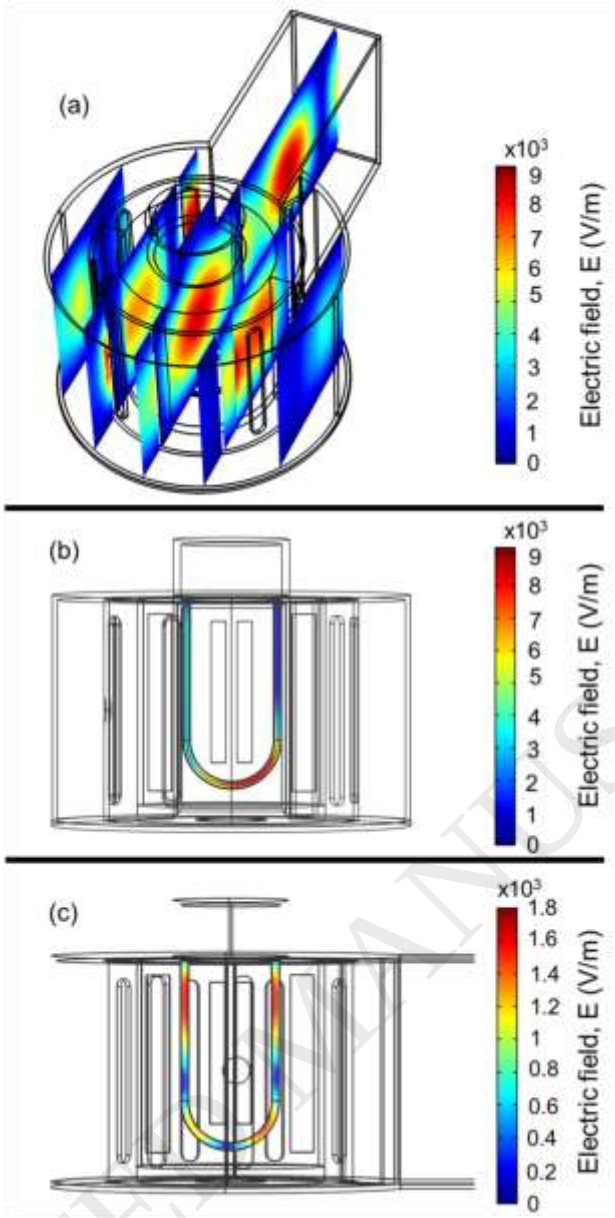

Figure 5. Electric field maps inside the (a) empty cavity and the tube for (b) parallel-to-port and (c) perpendicular-to-port tube orientation inside the microwave cavity. Flow rate, 0.7 ml/min; microwave power, 35 W; system pressure, 1 bara; frequency, 2.47 GHz.

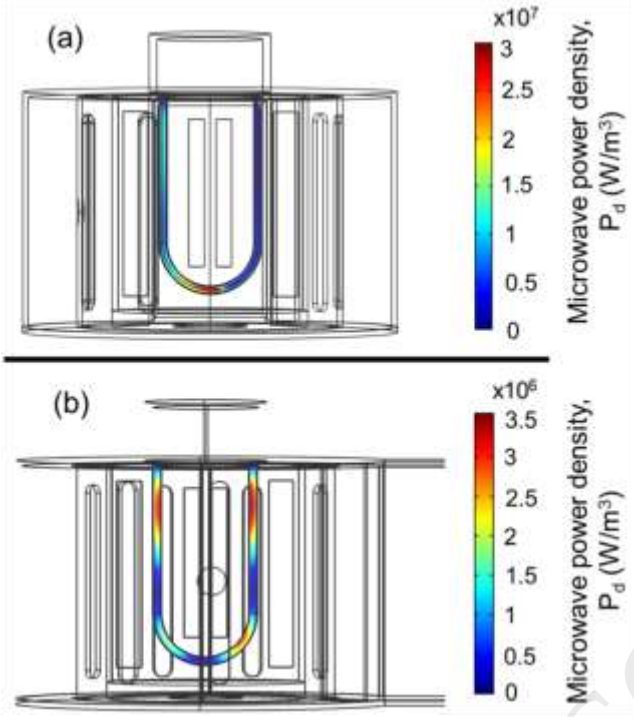

Figure 6. Microwave power density inside the tube for (a) parallel-to-port and (b) perpendicular-to-port tube orientation inside the microwave cavity. Flow rate, 0.7 ml/min; microwave power, 35 W; system pressure, 1 bara; frequency, 2.47 GHz.

4.1.3 Effect of inlet flow rate on temperature profile

Microwave heating is related to the volume of the workload (volume of the medium) under the electromagnetic radiation and consequently the volumetric flow rate or the residence time of the medium [16, 19]. The effect of medium velocity was studied by varying the inlet flow rate from 0.5 ml/min to 1.5 ml/min and the results are shown in Figure 7. It has previously been shown that increasing the flow rate of the medium results in decreasing temperature at the outlet, due to the volumetric nature of the microwave heating [28]. Salvi et al. [37] increased the tap water flow rate by 2–fold in a vertical tube, resulting in a gradually decreasing temperature in the centre of the tube. Our study examined the effect of residence time on the axial temperature profile by increasing the flow rate of water by 3-fold at atmospheric pressure, under constant microwave power at 35 W and parallel-to-port orientation. Decreasing the flow rate from 0.7 ml/min to 0.5 ml/min, we observed a small difference in the experimental results on the water temperature profile (Figure 7). This could be related to the similar electric field profile and consequently same microwave power density in the tube for these two conditions. On the other hand, decreasing the flow rate from 1.5 ml/min to 0.7 ml/min, the experimentally measured temperature at points 1- 3 increased by ~ 10 – 20 ^{o}C. With regards to the 1.5 ml/min flow rate experiment, the temperature close to the outlet (point 5) remained close to 100 ^{o}C, which is higher compared with the results obtained for 0.5 ml/min and 0.7 ml/min. The absorbed microwave energy was used to maintain the temperature near the boiling point and overcome the temperature drop

associated with heat losses due to conduction, radiation and microwaves reflection due to bubble generation.

The FEM model enabled us to trace the temperature profile at different flow rates. We also note that the difference between experimental and theoretical temperature profiles obtained at 0.5 ml/min and 0.7 ml/min flow rates was similar, further validating the model. For all flow rates studied, the temperature discrepancies between experiments and simulations were of the same order of magnitude, similar to the previous cases (Sections 4.1.1 and 4.1.2).

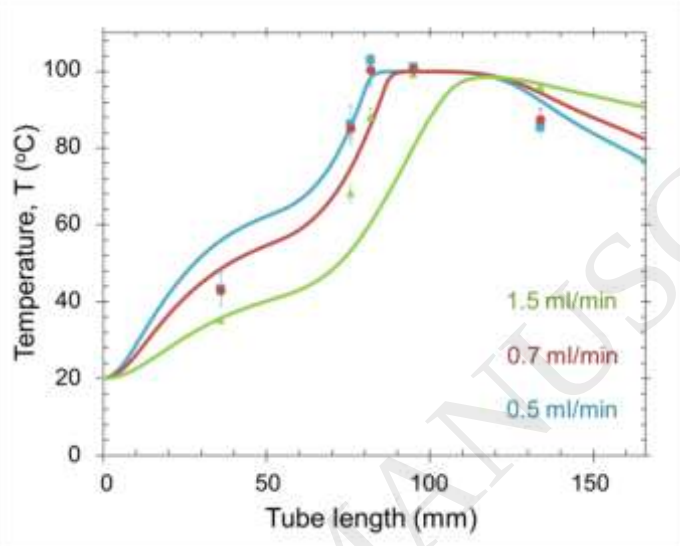

Figure 7. Experimental and computational results of the temperature profile inside the tube, when varying the flow rates. Microwave power, 35 W; tube orientation, parallel-to-port; system pressure, 1 bara; frequency, 2.47 GHz (marks: experimental results; lines: computational results). Error bars correspond to the standard deviation of three experimental measurements at each point. Computational results correspond to the temperature profile in the centre of the tube (water domain).

4.1.4 Effect of operating pressure on temperature profile

The temperature profile inside the tube was examined at higher pressure, 2.3 bara, and various microwave input powers. An important parameter which defines the dielectric properties is relaxation time and describes the rate of increase and collapse of polarisation [39, 40]. For polar liquids, relaxation time is a function of temperature and viscosity, as dipoles are affected and oriented by the random molecular movement due to the thermal motion [19]. Researchers developed empirical formulas describing the dielectric properties and relaxation times of water as a function of temperature for given microwave frequencies, while studies on polar solvents considered pressure as another variable [41-45]. The effect of pressure on the dielectric constant of polar solvents was attributed to the increased compression of the liquid under pressure [41, 45]. The study of Schornack and Eckert [41] showed the importance of system pressure on the dielectric properties of polar solvents.

Bradley and Pitzer [46] and Floriano and Nascimento [47] developed empirical correlations to relate the dielectric constant of water to the system temperature and pressure. These correlations show that there is an insignificant increase in the dielectric constant when increasing the pressure to 2.3 bara (see Table S2, Supplementary Information). Increasing the system pressure the boiling point increases; the boiling point of water is 125 ^{o}C at 2.3 bara. In order to simulate the system at 2.3 bara, the dielectric constant and dielectric loss of water were extrapolated from the experimentally measured properties at atmospheric pressure (see Figure S1, Supplementary Information). As described in Section 4.1.1, to account for the phase change above boiling point conditions, we assumed that the dielectric loss of water became zero, when the temperature reached 125 ^{o}C at 2.3 bara pressure. As bubbling was observed from 120 ^{o}C at 2.3 bara, the experimentally measured ε'' values were extrapolated only up to 120 ^{o}C. A linear interpolation was then performed between ε'' at 120 ^{o}C to $\varepsilon'' = 0$ at 125 ^{o}C by COMSOL.

Figure 8 shows computational results of the temperature profile throughout the tube length at 2.3 bara pressure. Although there was limited quantitative agreement between model and experiments for 5 W and 15 W under pressure, there was satisfactory agreement for 25 W. A temperature drop was observed at the tube outlet, similar to the results obtained at atmospheric pressure (1 bara). Comparing the experimental results shown in Figures 3 and 8, for the same input microwave power, there was a 3-15 ^{o}C temperature increase at 5 W and up to 20 ^{o}C increase at 15 W and 25 W, when increasing the pressure to 2.3 bara. The temperature difference was higher towards the middle and near the outlet of the tube, where rapid temperature increase and higher temperatures were observed. Nevertheless, the temperature profile remained qualitatively similar.

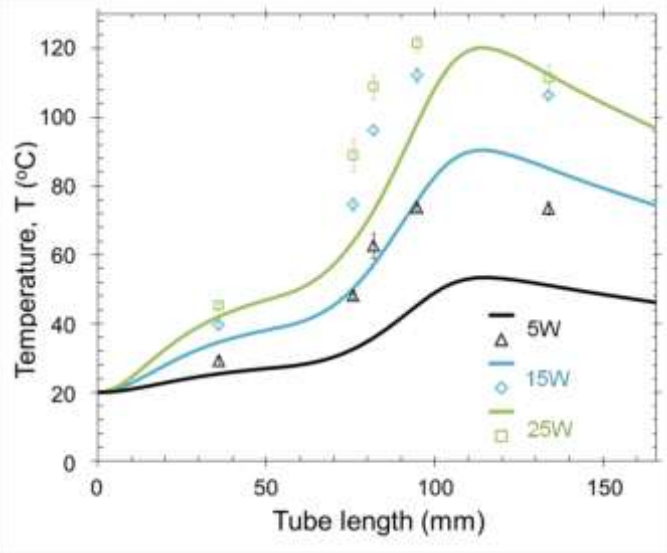

Figure 8. Experimental and computational results of the temperature profile inside the tube at 2.3 bara pressure, when varying microwave power in the range 5-25 W. Flow rate, 0.7 ml/min; tube orientation, parallel-to-port; frequency, 2.47 GHz (marks: experimental results, lines: computational results). Error bars correspond to the standard deviation of three experimental measurements at each point. Computational results correspond to the temperature profile in the centre of the tube (water domain).

4.2 Modelling of the electric field and absorbed power under microwave irradiation

The electric field inside the tube under microwave heating was simulated using the FEM model. The temperature profile was conjugated with the electric field profile, as the electromagnetic field governs the microwave absorbance and the observed temperature profile and vice versa, due to the dependency of the dielectric properties on temperature. Therefore, the developed model could offer an insight on the electromagnetics inside the tube and the energy balance of the system. A detailed discussion on the electric field profile and the absorbed microwave power is presented in the following sections.

4.2.1 Electric field and temperature profile in the tube

The electric field profile inside the cavity and tube is of major importance, as it is directly related to the microwave power density (Equation (2)). When the tube was placed in the cavity, it caused perturbation of the electric field. This perturbation was dependent on the geometry of the cavity and the dielectric properties of the materials, as well as the tube orientation, as previously discussed is Section 4.1.2. Figure 9 shows the electric field throughout the tube length, for parallel-to-port and perpendicular-to-port orientation. For parallel-to-port, there was an electric field maximum close to the middle of the tube. However, when the tube was placed perpendicularly to the applied field, the field fluctuated

around an average value (1 kV/m), affected by the field perturbation [31]. The electric field profile is also affected by the input microwave power. Figure 9 shows the electric field and theoretical temperature profile along the tube length for two input microwave powers (5 W and 35 W). For both cases, the temperature profile was not uniform (non-isothermal conditions) along the tube length, while water temperature increased rapidly and reached its maximum value around the middle of the tube, at ca. 90 mm, corresponding to the point where the curve of the tube was located and maximum electric field intensity was observed. Increasing the microwave power from 5 W to 35 W for parallel-to port orientation, the electric field intensity increased from 3.4×10^3 V/m (5 W) to 9×10^3 V/m (35 W) and the maximum temperature increased from ~ 55 ^{o}C (5 W) to ~ 100 ^{o}C (35 W).

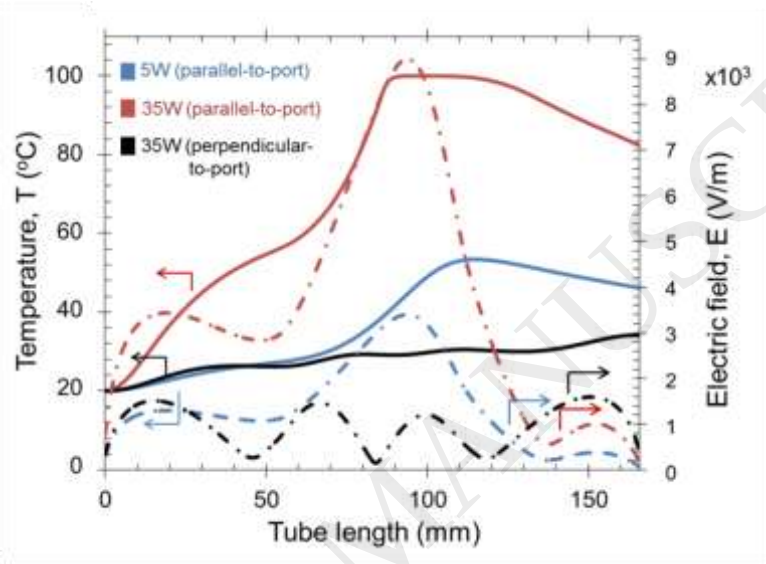

Figure 9. Computational results of the electric field and temperature profiles inside the tube for parallel-to-port orientation for 5 W and 35 W and for perpendicular-to-port orientation for 35 W. Flow rate, 0.7 ml/min; system pressure, 1 bara; frequency, 2.47 GHz (solid lines: temperature profile, dash dotted lines: electric field profile). Computational results correspond to the electric field and temperature profiles in the centre of the tube (water domain).

4.2.2 Effect of the process parameters on absorbed microwave power

The developed model allows the estimation of the power absorbed by the continuous flow system and evaluation of the desired process parameters for achieving the targeted temperature profile and minimising energy usage. The lack of monitoring of reflected power in the microwave cavity makes the computational model a necessary tool to estimate the energy required. The absorbed microwave power was calculated via volume integration of the tube [25], in the Step 2 of the computational methodology :

$$P_{total} = \iiint_V P_d \, dxdydz \tag{8}$$

where P_d is the microwave power density generated inside the tube and x, y, z are the respective coordinates.

Increasing the input microwave power to 20 W, the absorbed power reached 4.6 W. Further increase of the input power up to 35 W led to plateauing of the microwave absorption at 5 W, as it is a function of both the electric field intensity and the dielectric properties, which are temperature dependent. Therefore, given the temperature profile results in Figure 3a and Figure 3b, in which temperature increased by increasing the input power up to 20 W and it remained constant up to 35 W, increasing the input microwave power led to an excess of microwave power which could not be absorbed by the system (Table 1).

There was a dramatic decrease on the microwave absorbance from 8.7 W to 5 W, corresponding to 25 % and 14 % of absorbed over input microwave power, respectively, when decreasing the flow rate from 1.5 ml/min to 0.7 ml/min at 35 W microwave power. Decreasing the flow rate further to 0.5 ml/min resulted to further drop to 12 % in the absorbed over input microwave power ratio. These results demonstrate the enhancement of the microwave efficiency at higher flow rates which could be a result of water dielectric properties change and possible bubble formation due to evaporation, causing perturbation to the electric field. Increasing the water temperature, the dielectric properties decrease causing alterations to the field perturbations, while water at lower dielectric loss values couples weakly with the applied microwave field. On the other hand, for the case study of tube orientation (***D*** in Table 1) the absorbed microwave power for perpendicular-to-port orientation shows a 80 % decrease, as compared to parallel-to-port orientation, since parts of the U-tube coinciding with the minima and maxima of the applied electric field in resonant mode, affected the electric field profile and thereby the power density inside the tube. By increasing the pressure from 1 bara to 2.3 bara, the absorbed microwave power was unaffected, despite the significant temperature increase (***E*** in Table 1), indicating the need for accurate dielectric data of water under pressure.

Table 1. Absorbed microwave power by water inside the tube for different experimental conditions (values in parentheses display the percentage of the absorbed over the input microwave power).

Input microwave power, P_{in}	Absorbed microwave power P_{total} (W)				
	A	***B***	***C***	***D***	***E***
5 W		1.9 (38 %)			1.9 (38 %)
10 W		3.1 (31 %)			-
15 W	-	4.0 (27 %)	-	-	4.0 (27 %)
20 W		4.6 (23 %)			-
25 W		4.8 (19 %)			5.8 (23 %)
30 W		4.9 (16 %)			-
35 W	8.7 (25 %)	5.0 (14 %)	4.1 (12 %)	1.0 (3 %)	-

A*:* Flow rate, 1.5 ml/min; tube orientation, parallel-to-port; pressure, 1 bara; frequency, 2.47 GHz

B*:* Flow rate, 0.7 ml/min; tube orientation, parallel-to-port; pressure, 1 bara; frequency, 2.47 GHz

C*:* Flow rate, 0.5 ml/min; tube orientation, parallel-to-port; pressure, 1 bara; frequency, 2.47 GHz

D*:* Flow rate, 0.7 ml/min; tube orientation, perpendicular-to-port; pressure, 1 bara; frequency, 2.47 GHz

E*:* Flow rate, 0.7 ml/min; tube orientation, parallel-to-port; pressure, 2.3 bara; frequency, 2.47 GHz

5. Conclusions

In this work, microwave heating of water continuously flowing in a small diameter tube was investigated. Microwave power played a significant role in the temperature profile and temperature increase throughout the tube length. When increasing the input microwave power up to 20 W, the longitudinal temperature increased for the same axial position, due to the increasing absorbed microwave power. Further increase of the input microwave power up to 35 W, resulted in an insignificant increase in the temperature profile, since the electric field intensity increased only to a low extent and the absorbed power remained constant. Changing the orientation of the tube from parallel to perpendicular position towards the microwave port led to 50 ^{o}C decrease of the maximum temperature and 80 % reduction of the absorbed microwave power, due to perturbation of the electric field. Decreasing the water flow rate from 1.5 ml/min to 0.5 ml/min resulted in the same final maximum temperature; however, the microwave absorbance reduced dramatically by 53 % due to the volumetric nature of the microwave heating. Increasing the pressure from 1 bara to 2.3 bara, which raised the water boiling point to 125 ^{o}C, resulted in higher temperatures for the same microwave power, despite the same qualitative temperature profile. The results of the developed computational FEM model showed sufficient qualitative and quantitative agreement with experimental data, thereby establishing a robust methodology for tuning the

operating conditions of microwave-assisted reactors to trace the temperature and electric field profiles and calculating the power absorption.

6. Acknowledgements

The authors thank the EPSRC for financial support (EP/M015157/1) through the Manufacturing Advanced Functional Materials (MaFuMa) scheme.

7. References

[1] K.K. Rana, S. Rana, Microwave reactors: A brief review on its fundamental aspects and applications, Open Access Library Journal 1 (2014) 1-20.
[2] M. Matsuzawa, S. Togashi, S. Hasebe, Isothermal reactor for continuous flow microwave-assisted chemical reaction, Journal of Thermal Science and Technology 7 (2012) 58-74.
[3] M. Komorowska-Durka, G. Dimitrakis, D. Bogdał, A.I. Stankiewicz, G.D. Stefanidis, A concise review on microwave-assisted polycondensation reactions and curing of polycondensation polymers with focus on the effect of process conditions, Chemical Engineering Journal 264 (2015) 633-644.
[4] R.J.J. Jachuck, D.K. Selvaraj, R.S. Varma, Process intensification: oxidation of benzyl alcohol using a continuous isothermal reactor under microwave irradiation, Green Chem. 8 (2006) 29-33.
[5] M.L. Calabrese, G. d'Ambrosio, R. Massa, G. Petraglia, A high-efficiency waveguide applicator for in vitro exposure of mammalian cells at 1.95 GHz, IEEE Transactions on Microwave Theory and Techniques 54 (2006) 2256 - 2264.
[6] M.E.C. Oliveira, A.S. Franca, Microwave heating of foodstuffs, Journal of Food Engineering 53 (2002) 347-359.
[7] M. Baghbanzadeh, L. Carbone, P.D. Cozzoli, C.O. Kappe, Microwave-assisted synthesis of colloidal inorganic nanocrystals, Angew Chem Int Ed Engl 50 (2011) 11312-11359.
[8] M. Nishioka, M. Miyakawa, Y. Daino, H. Kataoka, H. Koda, K. Sato, T.M. Suzuki, Single-mode microwave reactor used for continuous flow reactions under elevated pressure, Industrial & Engineering Chemistry Research 52 (2013) 4683-4687.
[9] D. Bogdal, S. Bednarz, M. Łukasiewicz, W. Kasprzyk, Intensification of oxidation and epoxidation reactions—Microwave vs. conventional heating, Chemical Engineering and Processing: Process Intensification 132 (2018) 208-217.
[10] N.G. Patil, A.I.G. Hermans, F. Benaskar, J. Meuldijk, L.A. Hulshof, V. Hessel, J.C. Schouten, E.V. Rebrov, Energy efficient and controlled flow processing under microwave heating by using a millireactor-heat exchanger, AIChE Journal 58 (2012) 3144-3155.
[11] R. Cherbański, E. Molga, Intensification of desorption processes by use of microwaves—An overview of possible applications and industrial perspectives, Chemical Engineering and Processing: Process Intensification 48 (2009) 48-58.
[12] K. Werth, P. Lutze, A.A. Kiss, A.I. Stankiewicz, G.D. Stefanidis, A. Górak, A systematic investigation of microwave-assisted reactive distillation: Influence of microwaves on separation and reaction, Chemical Engineering and Processing: Process Intensification 93 (2015) 87-97.
[13] R. Cecilia, U. Kunz, T. Turek, Possibilities of process intensification using microwaves applied to catalytic microreactors, Chemical Engineering and Processing: Process Intensification 46 (2007) 870-881.
[14] G.S.J. Sturm, G.D. Stefanidis, M.D. Verweij, T.D.T. Van Gerven, A.I. Stankiewicz, Design principles of microwave applicators for small-scale process equipment, Chemical Engineering and Processing: Process Intensification 49 (2010) 912-922.
[15] G.S.J. Sturm, M.D. Verweij, A.I. Stankiewicz, G.D. Stefanidis, Microwaves and microreactors: Design challenges and remedies, Chemical Engineering Journal 243 (2014) 147-158.

[16] R. Meredith, Engineers' Handbook of Industrial Microwave Heating, The Institution of Engineering and Technology, London, 1998.
[17] N.G. Patil, F. Benaskar, J. Meuldijk, L.A. Hulshof, V. Hessel, J.C. Schouten, E.D.C. Esveld, E.V. Rebrov, Microwave assisted flow synthesis: Coupling of electromagnetic and hydrodynamic phenomena, AIChE Journal 60 (2014) 3824-3832.
[18] G. Link, V. Ramopoulos, Simple analytical approach for industrial microwave applicator design, Chemical Engineering and Processing: Process Intensification 125 (2018) 334-342.
[19] G.D. Stefanidis, A.N. Muñoz, G.S.J. Sturm, A. Stankiewicz, A helicopter view of microwave application to chemical processes: Reactions, separations, and equipment concepts, Reviews in Chemical Engineering 30 (2014) 233-259.
[20] G.S.J. Sturm, M.D. Verweij, T. Van Gerven, A.I. Stankiewicz, G.D. Stefanidis, On the effect of resonant microwave fields on temperature distribution in time and space, International Journal of Heat and Mass Transfer 55 (2012) 3800-3811.
[21] J. Zhu, A.V. Kuznetsov, K.P. Sandeep, Numerical modeling of a moving particle in a continuous flow subjected to microwave heating, Numerical Heat Transfer, Part A: Applications 52 (2007) 417-439.
[22] D. Salvi, D. Boldor, G.M. Aita, C.M. Sabliov, COMSOL Multiphysics model for continuous flow microwave heating of liquids, Journal of Food Engineering 104 (2011) 422-429.
[23] R. Cherbański, L. Rudniak, Modelling of microwave heating of water in a monomode applicator – Influence of operating conditions, International Journal of Thermal Sciences 74 (2013) 214-229.
[24] S. Tuta, T.K. Palazoğlu, Finite element modeling of continuous-flow microwave heating of fluid foods and experimental validation, Journal of Food Engineering 192 (2017) 79-92.
[25] J. Zhu, A.V. Kuznetsov, K.P. Sandeep, Mathematical modeling of continuous flow microwave heating of liquids (effects of dielectric properties and design parameters), International Journal of Thermal Sciences 46 (2007) 328-341.
[26] K.M. Huang, Z. Lin, X.Q. Yang, Numerical simulation of microwave heating on chemical reaction in dilute solution, Progress In Electromagnetics Research 49 (2004) 273–289.
[27] D. Salvi, D. Boldor, J. Ortego, G.M. Aita, C.M. Sabliov, Numerical modeling of continuous flow microwave heating: A critical comparison of COMSOL and ANSYS, J Microw Power Electromagn Energy 44 (2010) 187–197.
[28] T. Yousefi, S.A. Mousavi, M.Z. Saghir, B. Farahbakhsh, An investigation on the microwave heating of flowing water: A numerical study, International Journal of Thermal Sciences 71 (2013) 118-127.
[29] J. Robinson, S. Kingman, D. Irvine, P. Licence, A. Smith, G. Dimitrakis, D. Obermayer, C.O. Kappe, Electromagnetic simulations of microwave heating experiments using reaction vessels made out of silicon carbide, Phys Chem Chem Phys 12 (2010) 10793-10800.
[30] G.S.J. Sturm, A.Q. Van Braam Houckgeest, M.D. Verweij, T. Van Gerven, A.I. Stankiewicz, G.D. Stefanidis, Exploration of rectangular waveguides as a basis for microwave enhanced continuous flow chemistries, Chemical Engineering Science 89 (2013) 196-205.
[31] A.J.L. Morgan, J. Naylon, S. Gooding, C. John, O. Squires, J. Lees, D.A. Barrow, A. Porch, Efficient microwave heating of microfluidic systems, Sensors and Actuators B: Chemical 181 (2013) 904-909.
[32] J. Robinson, S. Kingman, D. Irvine, P. Licence, A. Smith, G. Dimitrakis, D. Obermayer, C.O. Kappe, Understanding microwave heating effects in single mode type cavities-Theory and experiment, Phys Chem Chem Phys 12 (2010) 4750-4758.
[33] G.S.J. Sturm, M.D. Verweij, T. Van Gerven, A.I. Stankiewicz, G.D. Stefanidis, On the parametric sensitivity of heat generation by resonant microwave fields in process fluids, International Journal of Heat and Mass Transfer 57 (2013) 375-388.
[34] COMSOL Inc, CFD Module Users Guide v 5.2a, (2016).
[35] D.R. Baghurst, D.M.P. Mingos, Superheating effects associated with microwave dielectric heating, Journal of the Chemical Society, Chemical Communications (1992) 674-677.

[36] A. Ferrari, J. Hunt, A. Stiegman, G.B. Dudley, Microwave-assisted superheating and/or microwave-specific superboiling (nucleation-limited boiling) of liquids occurs under certain conditions but is mitigated by stirring, Molecules 20 (2015) 21672-21680.
[37] D. Salvi, J. Ortego, C. Arauz, C.M. Sabliov, D. Boldor, Experimental study of the effect of dielectric and physical properties on temperature distribution in fluids during continuous flow microwave heating, Journal of Food Engineering 93 (2009) 149-157.
[38] M. Uematsu, E.U. Frank, Static dielectric constant of water and steam, Journal of Physical and Chemical Reference Data 9 (1980) 1291-1306.
[39] U. Kaatze, Complex permittivity of water as a function of frequency and temperature, Journal of Chemical & Engineering Data 34 (1989) 371-374.
[40] U. Kaatze, Reference liquids for the calibration of dielectric sensors and measurement instruments, Measurement Science and Technology 18 (2007) 967-976.
[41] L.G. Schornack, C.A. Eckert, Effect of pressure on the density and dielectric constant of polar solvents, The Journal of Physical Chemistry 74 (1970) 3014-3020.
[42] L.A. Dunn, R.H. Stokes, Pressure and temperature dependence of the electrical permittivities of formamide and water, Transactions of the Faraday Society 65 (1969) 2906-2912.
[43] B.B. Owen, R.C. Miller, C.E. Milner, H.L. Cogan, The dielectric constant of water as a function of temperature and pressure (1,2), The Journal of Physical Chemistry 65 (1961) 2065-2070.
[44] J.S. Rosen, Refractive indices and dielectric constants of liquids and gases under pressure, The Journal of Chemical Physics 17 (1949) 1192-1197.
[45] B.B. Owen, S.R. Brinkley, The effect of pressure upon the dielectric constants of liquids, Physical Review 64 (1943) 32-36.
[46] D.J. Bradley, K.S. Pitzer, Thermodynamics of electrolytes. 12. Dielectric properties of water and Debye-Hueckel parameters to 350 ^{o}C and 1 kbar, The Journal of Physical Chemistry 83 (1979) 1599-1603.
[47] W.B. Floriano, M.A.C. Nascimento, Dielectric constant and density of water as a function of pressure at constant temperature, Brazilian Journal of Physics 34 (2004) 38-41.